JGR Space Physics

RESEARCH ARTICLE
10.1029/2018JA025965

Special Section:
The Earth's Magnetosphere: New Tools, New Thinking, New Results

Multisatellite Analysis of Plasma Pressure in the Inner Magnetosphere During the 1 June 2013 Geomagnetic Storm

M. Stepanova[1], E.E. Antonova[2,3], P.S. Moya[4], V.A. Pinto[5], and J.A. Valdivia[4,6]

[1]Physics Department, Universidad de Santiago de Chile, Santiago, Chile, [2]Skobeltsyn Institute of Nuclear Physics, Lomonosov Moscow State University, Moscow, Russia, [3]Russian Space Research Institute, Russian Academy of Sciences, Moscow, Russia, [4]Physics Department, Universidad de Chile, Santiago, Chile, [5]Department of Atmospheric and Oceanic Sciences, University of California, Los Angeles, CA, USA, [6]Center for the Development of Nanoscience and Nanotechnology, CEDENNA, Santiago, Chile

Key Points:
- We perform a multisatellite analysis of variation of plasma pressure in the magnetosphere during storm
- Plasma pressure inside the magnetosphere is mainly controlled by the solar wind dynamic pressure
- Radial pressure profiles change during the storm depending on it strength

Correspondence to:
M. Stepanova,
marina.stepanova@usach.cl

Citation:
Stepanova, M., Antonova, E. E., Moya, P. S., Pinto, V. A., & Valdivia, J. A. (2019). Multisatellite analysis of plasma pressure in the inner magnetosphere during the 1 June 2013 geomagnetic storm. *Journal of Geophysical Research: Space Physics*, *124*. https://doi.org/10.1029/2018JA025965

Received 2 AUG 2018
Accepted 16 JAN 2019
Accepted article online 28 JAN 2019

Abstract Using data from Defense Meteorological Satellite Program 16–18, National Oceanic and Atmospheric Administration 15–19, and METOP 1–2 satellites, we reconstructed for the first time a two-dimensional statistical distribution of plasma pressure in the inner magnetosphere during the 1 June 2013 geomagnetic storm with time resolution of 6 hr. Simultaneously, we used the data from Van Allen Probes and Time History of Events and Macroscale Interactions missions to obtain the in situ plasma pressure in the equatorial plane. This allowed us to corroborate that the dipole mapping works reasonably well during the storm time and that variations of plasma pressure are consistent at low and high altitudes; namely, we observed a drastic increase in plasma pressure a few hours before the storm onset that continued during the storm main phase. Plasma pressure remained elevated during the first 18 hr of the recovery phase and then started to decrease to normal levels. We found that the variation in pressure correlates with the change in the slope of the D_{st} index, and that the plasma pressure nearly conserved its axial symmetry during the storm, giving one more evidence that the ring current provides the main contribution to the D_{st} variation. We also found that the plasma pressure in the magnetosphere correlates with the solar wind dynamic pressure with a correlation coefficient exceeding 0.9, which can be related to the pressure balance at the magnetospheric flanks. The results obtained here agree with the concept of the ring current generation by an inner magnetosphere plasma ring in magnetostatic equilibrium.

Plain Language Summary We study the evolution of plasma pressure in the Earth's magnetosphere during strong geomagnetic storm. It is found that the pressure strongly increases during pre–storm time, and the main phase of storm. It starts to decrease during the recovery phase. These changes are driven by the solar wind dynamic pressure.

1. Introduction

There is plenty of evidence that plasma in the Earth's magnetosphere is in magnetostatic equilibrium; that is, the plasma pressure gradient is compensated by Ampere's force. This equilibrium remains true when the plasma velocity is much smaller than the sound and Alfvén speed and holds even in the presence of a high level of turbulence. Such feature of magnetospheric dynamics differs from the commonly observed picture in laboratory thermonuclear devices, where the development of instabilities leads to a quick destruction of the magnetostatic equilibrium and hence to the destruction of the plasma configuration that existed before the appearance of turbulence. How the magnetosphere reaches magnetostatic equilibrium and what specific conditions are necessary to maintain it are not yet fully understood. Unraveling these processes requires knowledge about the 2-D distribution of the plasma pressure for different geomagnetic conditions, as well as the understanding of the role of the external boundary conditions imposed by the solar wind flow and interplanetary magnetic field (IMF). The magnetostatic approach is also valid during geomagnetic storms and is useful to describe large-scale processes despite the comparatively medium-scale fluctuations of the plasma and magnetic field. This fact is reflected on the successful estimation of D_{st} from the Dessler-Parker-Sckopke relation and in the efforts to develop storm models (e.g., Ganushkina et al., 2010, 2015, 2018; Liemohn et al., 2001; Zaharia et al., 2005) and later works (Gkioulidou et al., 2014, 2016; Kistler et al., 2016; Zhao et al., 2015,

2016). Nevertheless, the mechanisms by which the plasma is able to maintain the magnetostatic equilibrium during storms is not clear. Therefore, it is important to study the behavior of the plasma pressure in the inner magnetosphere during both quiet times, and during the main and recovery phases of a geomagnetic storm.

Previous studies of plasma pressure can be divided into statistical studies and analysis of plasma pressure profiles. They can also be divided into studies of pressure using in situ data from high-altitude satellites, and studies using low-orbiting satellites with a subsequent mapping to the equatorial plane using empirical models of the geomagnetic field. Statistical studies of plasma pressure distribution in the inner magnetosphere using in situ measurements have been presented in several works. For example, Lui and Hamilton (1992) obtained average profiles of plasma pressure for different levels of geomagnetic activity using particle measurements onboard the high-altitude AMPTE/CCE satellite. Using data from the same satellite, De Michelis et al. (1997) showed that the distribution of plasma pressure around the Earth is nearly azimuthally symmetric, and the pressure gradients are mainly directed toward Earth. Wang et al. (2011) not only analyzed the spatial distributions of ion and electron fluxes using the Time History of Events and Macroscale Interactions (THEMIS) satellite data but also calculated the plasma pressure anisotropy and showed that the plasma pressure is nearly isotropic along the noon-midnight and the dawn-dusk meridians at geocentric distances $> 5R_E$, where R_E is the Earth's radius. Kirpichev and Antonova (2011) and Antonova et al. (2013) studied the distribution of plasma pressure at geocentric distances $< 15R_E$ and showed the existence of a ring-shaped structure surrounding the Earth using the data from the five THEMIS satellites. This structure forms the outer part of the ring current (RC) region. Antonova et al. (2013) also found that for any orientation of the IMF, the plasma pressure distribution is nearly axially symmetric, and for distances $> 6R_E$ the plasma pressure is nearly isotropic. Antonova and Kirpichev (2014) obtained the characteristics of plasma pressure using a more extensive THEMIS database and calculated the distribution of the plasma beta parameter in the inner magnetosphere.

The plasma pressure distribution in the equatorial plane can also be obtained from low-altitude polar-orbiting satellites under the assumption that the plasma pressure is conserved along a magnetic field line. In particular, Wing and Newell (1998, 2000) obtained the statistical distribution of plasma pressure at the equatorial plane using the Defense Meteorological Satellite Program (DMSP) satellites data. Wing et al. (2013) obtained the plasma pressure distribution at ionospheric altitudes for different phases of substorms. They showed that the presence of substorms increases the ion pressure by only 30%.

There are two main difficulties in the analysis of plasma pressure obtained from the low-altitude satellite data, namely, the accurate mapping between the equatorial plane and ionospheric altitudes and the influence of the field-aligned potential drop, specifically, the use of different models of geomagnetic field produce very different mappings between the ionosphere and the equatorial plane (e.g., Stepanova et al., 2006, 2008). Similarly, the existence of field-aligned potential drops at auroral field lines leads to a decrease in the plasma pressure at low altitudes in the region of upward field-aligned current. Stepanova et al. (2006, 2008, 2004, 2002) developed a methodology to consider the influence of field-aligned potential drops on the plasma pressure and showed that such correction may increase the value of plasma pressure a few times, depending on the value of the potential drop and the ion temperature.

A correct determination of the values of plasma pressure both in the equatorial plane and at low altitudes is very important considering that these values may be used as a "natural tracer" for the mapping of the auroral oval into the equatorial plane. Using this methodology, Antonova et al. (2014, 2015) found that a considerable part of the auroral oval can be mapped into a ring-shaped structure surrounding the Earth. The values of the plasma beta parameter inside the ring are of the order of unity, indicating that the ring-shaped structure is an important constituent of the magnetospheric current system and play an active role in the magnetic field distortion. This result is very important for the analysis of the dynamics of geomagnetic storms and substorms. To date, there are some important studies about the behavior of plasma pressure inside the magnetosphere during geomagnetic storms. For example, Zhang et al. (2007) compared the evolution of the main plasma parameters and of the geomagnetic field, as observed by the Los Alamos National Laboratory geostationary satellites, with the Space Weather Modeling Framework during the 19 May 2002 geomagnetic storm, including the variation of plasma pressure. It was found that the model reproduces the main features of the plasma pressure, including its strong increase during the main phase in the night sector (e.g., see Figure 8 of Zhang et al., 2007).

Measurements of the energetic neutral atom (ENA) fluxes provide a snapshot of a global ion population in the magnetosphere and have been successfully used for the study of storm time plasma signatures. For example, Denton et al. (2005) analyzed the data of the medium energy neutral atom imager at energies of 6 and 12 keV around D_{st} minimum time of the 21 October 2001 GEM IM-S challenge storm and found that the peak in ENA emissions for these energies is located close to midnight and its radial location varies from $\sim$ 2 to $\sim$ $5R_E$ and does not show any systematic behavior. Therefore, it is possible to take this result as an indication that at the end of a storm's main phase the ion pressure may have a maximum close to midnight. There are, however, a long list of assumptions to be fulfilled when obtaining the ion pressure from the neutral atom fluxes. The most common is the inverse approach that obtains the ion fluxes in some energy range from the simulation of the ion drift in modeled large-scale electric and magnetic fields, and to compare them with the ENA observations (e.g., see Ebihara & Fok, 2004). Some works use a more sophisticated approach combining an existing global magnetohydrodynamic and a kinetic RC model (e.g., see Buzulukova et al., 2010). The plasma pressure profiles obtained are usually strongly dependent on the specific models used and how they are combined (e.g., see Figure 5 of Buzulukova et al., 2010). This means that the knowledge about the real 2-D distribution of plasma pressure and its evolution during a storm is very important for the validation of the results of the modeling of plasma pressure in the inner magnetosphere.

To date, there are no studies about the azimuthal distribution of the plasma pressure obtained simultaneously across several magnetic local time (MLT) during storm phases, and the possible influence of the solar wind parameters on the radial and azimuthal distribution. According to Antonova et al. (2018) there is strong evidence that the majority of the auroral oval is mapped into the plasma ring surrounding the Earth. The radial plasma pressure gradients in this ring, denominated the Cut-Ring-Current (CRC) by Antonova and Ganushkina (1997), generates the high-latitude continuation of the ordinary RC. The contribution of this current into the D_{st} variation could be important to take into account, since the volume of the magnetic flux tubes at those distances is considerably large so that even a relatively small increase in plasma pressure could generate a strong CRC. This effect could be even stronger when the plasma pressure increases due to changes in the solar wind parameters; however, its effect has not been studied in detail so far. Stepanova et al. (2008) analyzed the plasma pressure profiles in the magnetosphere during the 1 March 1982 geomagnetic storms and found that the maximum value of pressure (obtained using the data from the DMSP satellite along a satellite orbit) correlates with the solar wind dynamic pressure. Another important point is the contribution of oxygen to the plasma pressure during storms. There are many evidences that the level of oxygen in the magnetosphere significantly increases during a magnetic storm. For example, recently, Kistler et al. (2016) analyzed the 1 June 2013 storm and showed that although the energy density of both H^+ and O^+ increases significantly prior to the start and during the main phase of the storm, the contribution of O^+ to the plasma pressure was essential. To date, it is considered that the auroral oval is one of the main sources of O^+ during storms; however the exact role of the O^+ in the storm dynamics is not clear. This is one of the reasons, why we used the same storm as Kistler et al. (2016).

In this work we present a comprehensive study of the dynamics of the plasma pressure in the inner magnetosphere during the same 1 June 2013 storm analyzed by Kistler et al. (2016). Our study is based on the simultaneous use of the data of both high altitude in situ measurements obtained by the THEMIS (Angelopoulos, 2008) and Van Allen Probes (Mauk et al., 2012) missions, and the data from the low-orbiting DMSP and Polar Operational Environmental Satellites (POES) spacecraft and shows how the pressure changes in the inner magnetosphere before and during the storm in response to the changes in the solar wind dynamic pressure. The paper is organized as follows: section 2 discusses the instrumentation and data analysis of the DMSP, POES, Van Allen Probes, and THEMIS missions. Section 3 presents the detailed analysis of the variation of plasma pressure during the 1 June 2013 storm. Section 4 contains the discussion about the role of the variation of plasma pressure in the development of the storm, and section 5 is dedicated to conclusions.

2. Instrumentation and Data Analysis

The simultaneous use of low- and high-orbiting satellites attempts to shorten the gap between the in situ measurements near the equatorial plane and the measurements done by low-orbiting satellites, all to obtain the main features of the plasma pressure behavior during a geomagnetic storm.

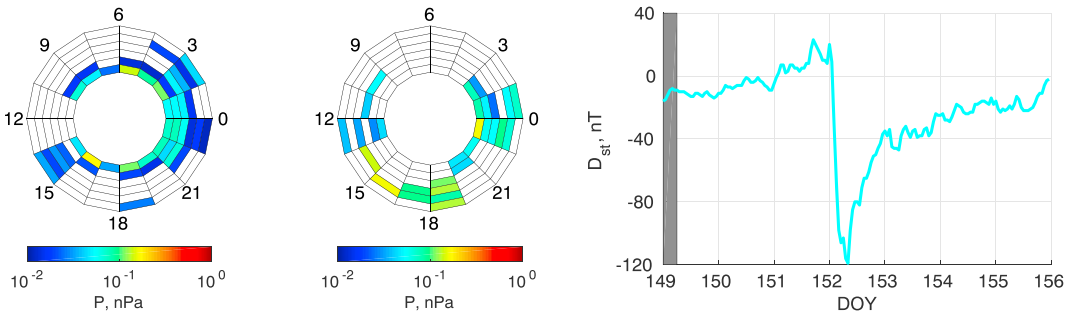

Figure 1. The 2-D distribution of the plasma pressure from the Defense Meteorological Satellite Program (left) and Polar Operational Environmental Satellites (right) satellites averaged during 6 hr between 0 and 6 UT on 29 May 2013 (DOY 149). The time interval is indicated as a gray band in the D_{st} graph on the right of both pressure distributions. The D_{st} index was taken from the 1-hr resolution OMNI database. DOY = day of year.

2.1. Low-Orbiting Satellite Data Processing

We used the data of the F16-F18 DMSP spacecraft, and the satellites NOAA 15-19 and METOP 1-2 of the NOAA/POES mission. The satellites of both missions have nearly circular solar-synchronous polar orbits with altitudes of ~ 840 km. To calculate the plasma pressure from the ion precipitating particle fluxes, in the case of the DMSP data we used the methodology developed by Stepanova et al. (2006, 2008, 2004, 2002) for quiet periods and during magnetic storm events. This methodology considers the effects of the field-aligned potential drop on the ion precipitations. However, for this particular study we are interested in comparing the results of both low-altitude missions. Thus, as the POES satellite does not provide the electron spectra with enough energy resolution for the detection of the potential drop, we used the pressure values obtained without considering this correction. The ion plasma pressure was calculated using the data of ion precipitating fluxes measured by the SSJ/4 electrostatic analyzer (ESA). For this study we restricted the ion energy range to 0.139–20.4 keV, which was established after the processing on tens of thousands of spectra as a most suitable energy range for an automatic data processing.

In the case of the POES satellites, the data of the Total Energy Detector were used. The proton differential flux is publicly available in https://www.ngdc.noaa.gov/stp/satellite/poes/dataaccess.html for the energies of 0.189, 0.844, 2.595, and 7.980 keV only, limiting the scope of our study, but allowing the possibility to use the data of seven satellites at the same time. Therefore, we compared the obtained results with the pressure values obtained using the data of DMSP satellites. The values of plasma pressure for POES satellites were obtained by direct integration of the proton flux J as a function of energy E, and also by the linear fit of $\ln(J(E)/E)$, that allowed us to obtain the values of the ion number density (n) and temperature (T), and hence, the plasma pressure ($p = 0.16\, n\, T$, where n is measured in per cubic centimeters, T is measured in kiloelectron volts, and p is measured in nanopascals). Only the values for which the difference between the pressures obtained by both methods was less than 50% were considered.

It is well known that ions are the main contribution to the plasma pressure in the inner magnetosphere, while the electron contribution to the plasma pressure at the equatorial plane is only ~ 14–17%. Together with the limited range of ion energy, as well as the nonconsideration of the field-aligned potential drop, all these factors indicate that the true value of the plasma pressure should be higher than the value calculated following the present technique. It is important to mention that the use of the precipitating ion fluxes measured by low-orbiting satellites for the determination of plasma pressure implies the nearly isotropic ion distribution function. Fortunately, at the latitudes of the auroral oval the ion distribution functions are close to isotropic especially during magnetic storms (see, e.g., Greenspan & Hamilton, 2000).

All pressure data were divided into (L, MLT) bins, covering the radial distance between 7 and 13 R_E with the step of $\Delta L = 1\, R_E$, and the 0–24 MLT range with the step of Δ MLT = 1.5 hr. Here $L = \cos^{-2}(\mathrm{MLAT})$; MLAT is the geomagnetic latitude, and MLT is the magnetic local time. Although this mapping does not reflect all features of the near-Earth magnetic field, and its evolution during storms, it permits to analyze the ion pressure in the whole region surrounding the Earth plasma ring, leaving a more careful analysis for future studies. In this study the plasma pressure was obtained by automatic processing of the precipitating fluxes; therefore, we restricted the minimum radial distance to 6 R_E, to reduce the contamination of the results by energetic particles and also to ensure that the precipitating ion fluxes are originated in the regions

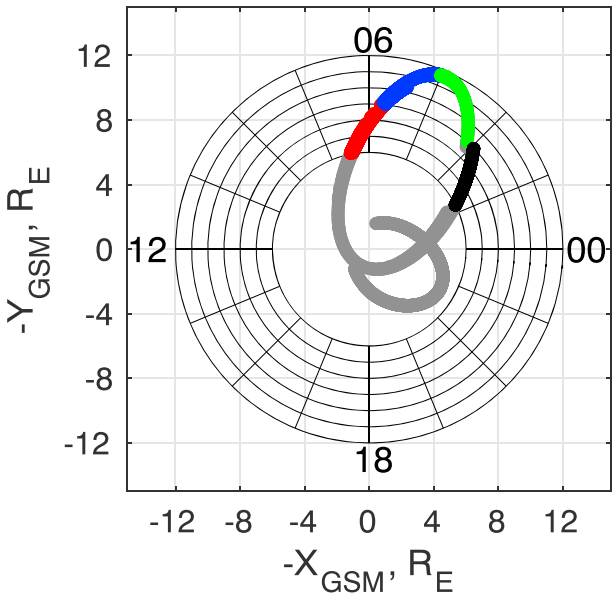

Figure 2. The orbits of the Time History of Events and Macroscale Interactions and Van Allen probe satellites. The red, blue, green, and black colors indicate the segments of the orbits used in the subsequent analysis. GSM = geocentric solar magnetospheric coordinates.

of the magnetosphere where the plasma pressure is nearly isotropic (see, e.g., Antonova & Kirpichev, 2014; De Michelis et al., 1997; Wang et al., 2011; recent results of Antonova et al., 2018, and references therein). It is worth mentioning that there could be asymmetry in precipitations from both hemispheres. The real configuration of the geomagnetic field deviates from a dipole field configuration, especially during storms. However, for this study we focused only on the global effects of the plasma pressure behavior during storm and used the (L, MLT) coordinates system instead of the (MLAT, MLT) to facilitate a direct comparison between the low-orbiting and high-orbiting data.

Figure 1 shows the 2-D distributions, obtained for the DMSP (left polar plot) and POES (right polar plot) satellite missions on 29 May 2013 (day of year, DOY, 149), between 0 and 6 UT. This time interval is indicated as a gray band in the right panel showing the D_{st} variation during the 1 June 2013 geomagnetic storm. As it can be seen in Figure 1, the values of pressure obtained from both missions do not differ significantly, yet, we will be processing all data separately to show the robustness of the procedure on any low-orbiting mission having onboard an ESA for the study of plasma pressure in the inner magnetosphere.

2.2. High-Orbiting Data Processing

To obtain the in situ plasma pressure near the equatorial plane, we used the data from the THEMIS and Van Allen Probes missions. The THC, THD, and THA satellites were in similar orbit with an apogee of approximately 12 R_E, located near to 4 MLT. The apogee of the Van Allen satellites was approximately 5.5 R_E and located near to 23 MLT (see Figure 2). To compare the statistical picture of plasma pressure from the DMSP/POES satellites and the plasma pressure from the THEMIS satellites, the THEMIS orbits were divided into four segments, indicated by black, green, blue, and red colors, for each of which the average plasma pressure was calculated for the same time intervals as in the case of the DMSP/POES data processing.

In the case of the THEMIS measurements we used the Level 2 ion pressure tensor data, provided by the THEMIS ESA instrument, which measures ions over the energy range from a few electron volts up to 25 keV (McFadden et al., 2008). For the Van Allen Probes mission, we used the data of the Energetic Particle Composition and Thermal Plasma Suite (Spence et al., 2013) Helium, Oxygen, Proton, and Electron (HOPE) instrument (Funsten et al., 2013), which provides number density and the temperature tensor for protons and ions separately, by measuring each specie in the energy range from 0.03 to 50 keV. For this study we used the scalar values of plasma pressure (obtained from the trace of the tensor) for both missions and did not consider the pressure anisotropy. The DMSP, POES, and THEMIS satellites did not carry instruments able to measure the ion composition; therefore, for this specific study we used the proton data only, in order to compare the pressure from different spacecraft. However, according to Kistler et al. (2016), the contribution of the O^+ ions to the energy density (pressure) was very important during the storm event. Therefore, we also analyzed how the inclusion of heavy ions affects the total plasma pressure using the data of the Van Allen Probe mission only.

2.3. The 1 June 2013 Geomagnetic Storm

During the 1 June 2013 geomagnetic storm, the provisional D_{st} index reached the minimum value of −119 nT at 09:00 UT on June 1 2013. Figure 3 shows the main solar wind parameters from the OMNI database for that particular event. As discussed by Keesee and Scime (2015), the storm was originated by a combination of a coronal mass ejection and a high-speed stream. The solar wind velocity more than doubled from less than 400 km/s (before storm and during the main phase) to nearly 800 km/s (during the recovery phase). The number density and the dynamic pressure strongly increased after 16:00 UT on 31 May 2013, that is, ~ 8 hr before the beginning of the main phase, reaching 25 cm^{-3} and 10 nPa, respectively. A sharp increase in the dynamic pressure caused an increase of the pressure at the magnetopause and the subsequent compression of the magnetosphere (see also first two panels in Figure 6). Both the number density and dynamic pressure maintained high values during the storm main phase and early recovery phase. Then, the dynamic pressure dropped and remained nearly constant. During the main phase the B_z component of the IMF turned

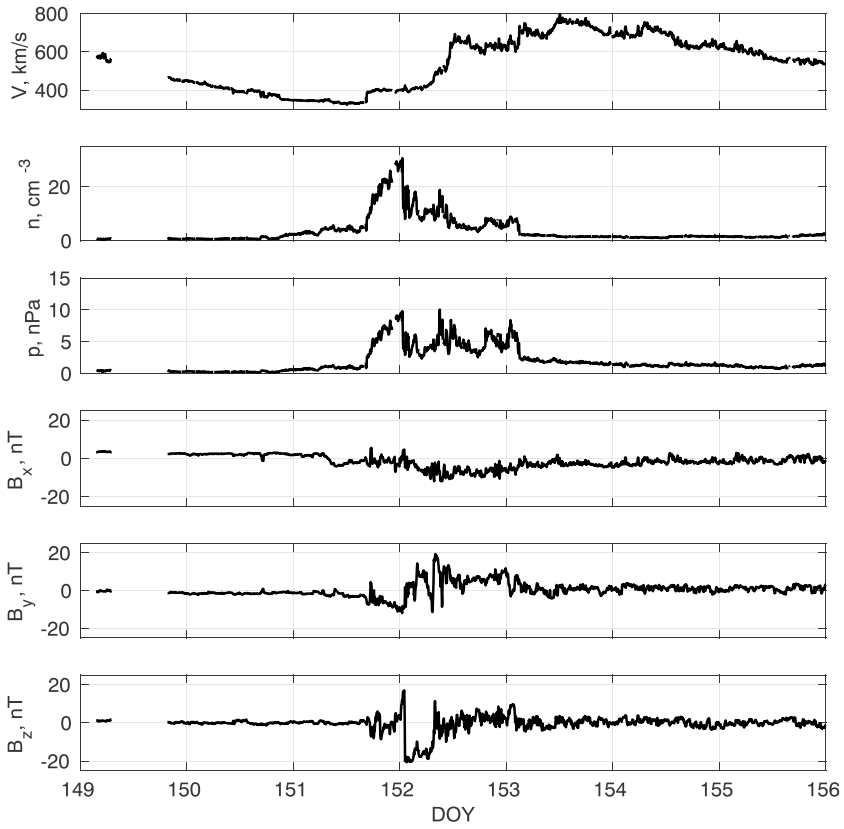

Figure 3. From top to bottom: The solar wind velocity, number density, dynamic pressure, and the three interplanetary magnetic field components for the 1 June 2013 geomagnetic storm from the 5-min resolution OMNI database. DOY = day of year.

southward and remained around -20 nT for about 7 hours in 1 June 2013, between 01:00 and 08:00 UT. After 08:00 UT, IMF B_z turned positive, reaching 10 nT in two opportunities, and oscillating between −5 and +5 nT, approximately during the next 3 days.

3. Variation of Plasma Pressure During the 1 June 2013 Geomagnetic Storm.

3.1. Two-Dimensional Variation of Plasma Pressure From Low-Orbiting Satellite

Figure 4 shows the 2-D distributions of plasma pressure obtained using the data of DMSP and POES satellite every 6 hr. As it can be seen, the values of pressure started to increase on 31 May 2013 between 18 and 24 UT and remained at high levels during 1 June 2013. Although the spatial coverage of the obtained pressure distribution is not uniform due to the solar-synchronous orbits of the satellites of both missions, the coverage was enough to detect the absence of a strong azimuthal asymmetry during both quiet and storm time intervals. Time to time it is possible to observe local increases of plasma pressure at different (L, MLT) sectors, but we did not detect any systematic pattern. Considering the fact that each 2-D distribution was obtained every 6 hr, it is not possible to argue whether these local increases have a spatial or temporal nature. We can only assure that a dramatic increase of pressure is observed for all L and MLT and that it started on 31 May 2013 between 18:00 and 24:00 UT and finished at the beginning of 2 June 2013.

3.2. Variation of Plasma Pressure From THEMIS Satellite for the Distances $7 < L < 13$

Figure 5 shows some examples of the variation of pressure along a THEMIS satellite trajectory before and during the 1 June 2013 geomagnetic storm. As in case of the DMSP/POES missions a sharp increase in the pressure is observed 6 hr before the beginning of the storm. To be able to make a quantitative comparison between the plasma pressure, obtained by the DMSP and POES satellites with the plasma pressure, measured near the equatorial plane, we averaged the pressure of the THEMIS THC, THD, and THA satellites every 6 hr for each of the four segments indicated in Figure 2. We also calculated the average pressure over all (L, MLT) bins, obtained by each low-orbiting mission (see Figure 4).

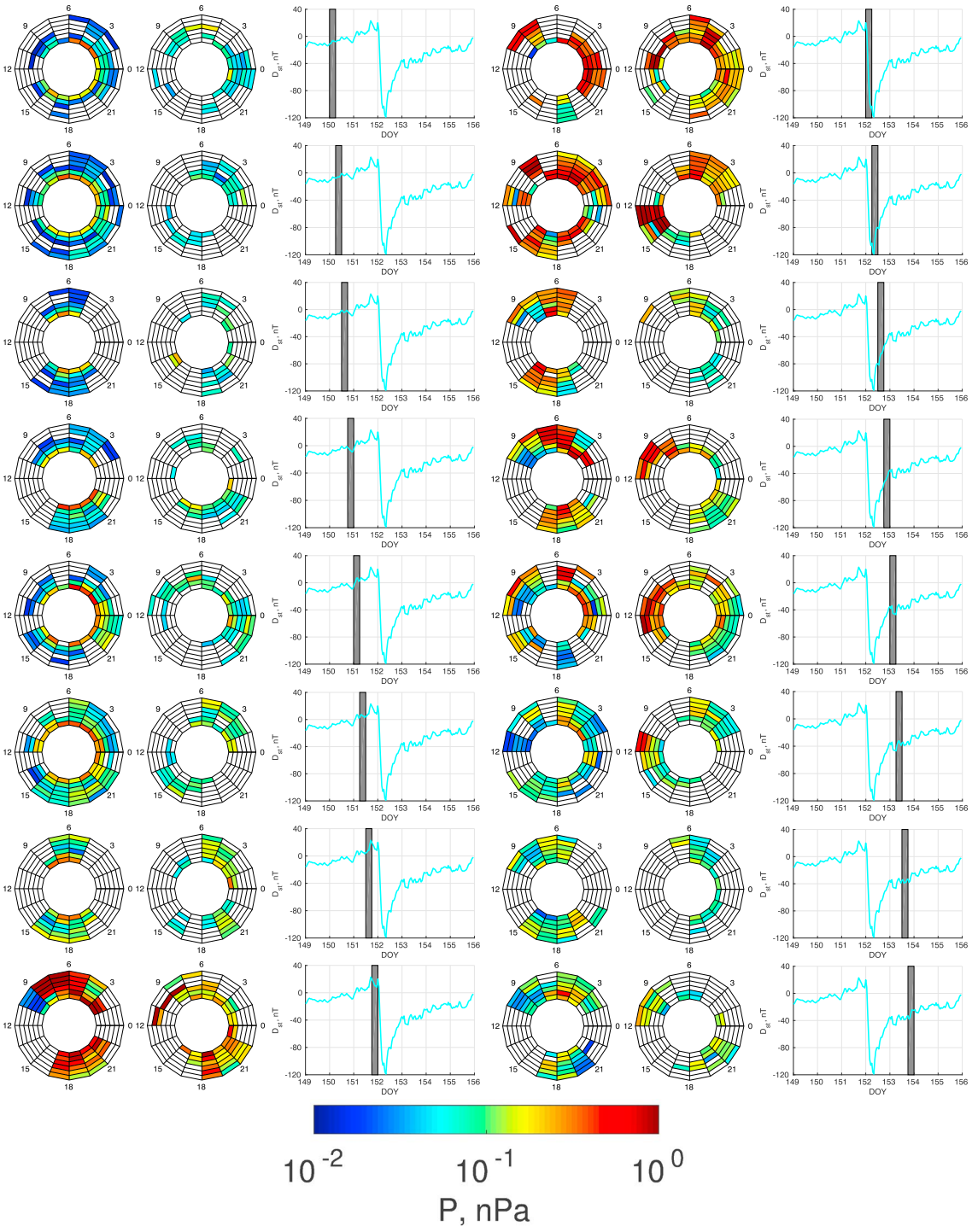

Figure 4. The 16 plots of 2-D distribution of plasma pressure obtained the same way as shown in Figure 1 between 30 May 2013 (DOY 150) and 2 June 2013 (DOY 153). The exact time interval is indicated as a green line in the D_{st} graph on the right of the pressure distributions. The color bar is the same as in Figure 1. DOY = day of year.

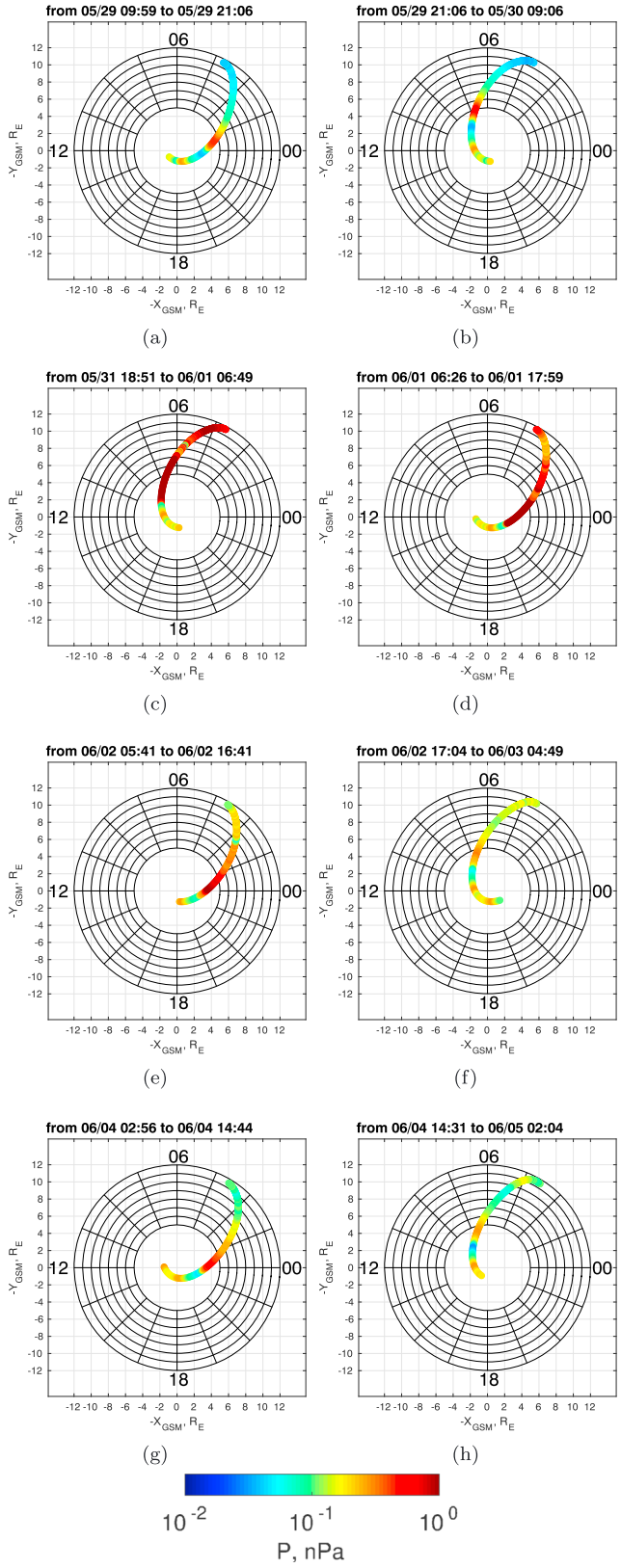

Figure 5. Examples of the variation of plasma pressure along a Time History of Events and Macroscale Interactions satellite trajectory for some inbound and outbound passages during quiet time (a, b), the main (c, d), and recovery (e–h) phases. The colors are the same as in Figures 1 and 2. GSM = geocentric solar magnetospheric coordinates.

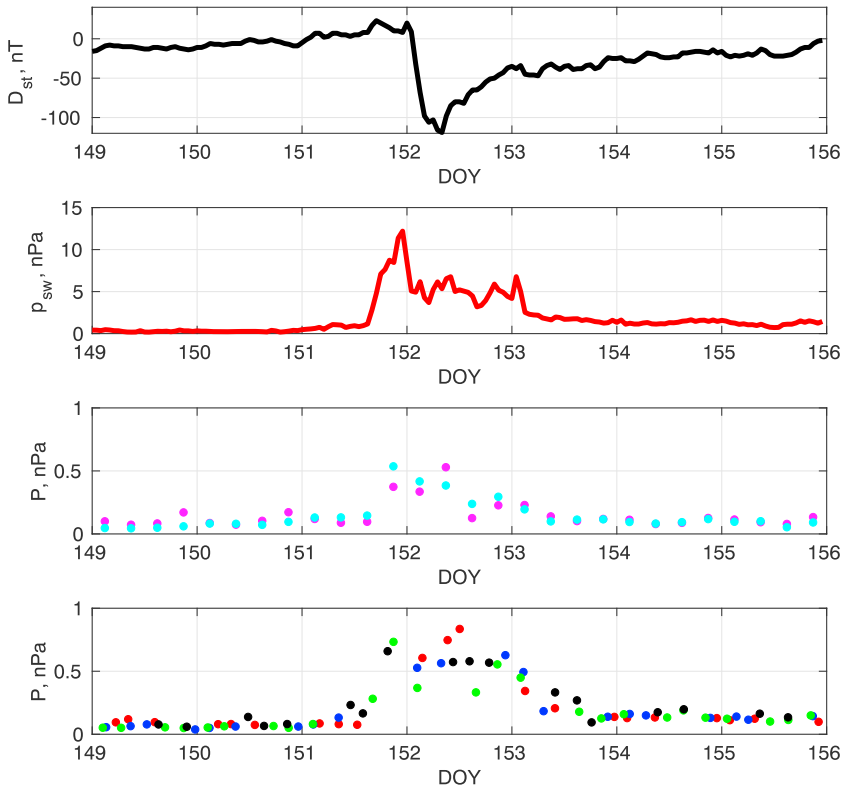

Figure 6. From top to bottom: The D_{st} index, the solar wind dynamic pressure, the plasma pressure from Defense Meteorological Satellite Program (cyan) satellite and Polar Operational Environmental Satellites (magenta), and the plasma pressure from Time History of Events and Macroscale Interactions satellites (the red, blue, green, and black colors indicate the segments of the orbit shown in Figure 2). DOY = day of year.

Figure 6 summarizes the obtained pressure variations during the 1 June 2013 storm. It also shows the variations in the solar wind dynamic pressure and D_{st} index. As it can be seen, the plasma pressures obtained from the DMSP (cyan) and POES (magenta) satellites (third panel top to bottom) and the pressures obtained from the THEMIS satellites for the four different segments (fourth panel) correlate very well with each other. They start to increase 6 hr before the storm and maintain high values during the main phase. They start to decrease during the recovery phase at the beginning of 2 June 2013 (DOY 153). It is interesting to notice that at the same time the D_{st} index changes its slope.

The most surprising fact is that the plasma pressure in the inner magnetosphere seems to correlate very well with the solar wind dynamic pressure. To prove this fact, we calculated the correlation coefficients between the dynamic pressure and the plasma pressures, obtained by each satellite mission. As it can be seen in Figure 7, the obtained correlation coefficients are very high: 0.97 for DMSP, 0.82 for POES, and 0.98 for THEMIS pressures, respectively. For this calculation we did not separate the THEMIS data into four segments and calculated the 6-hr-averaged value using all data between 7 and 13 R_E. As it can be seen, the lowest coefficient was obtained for the POES satellite mission. It is not too surprising considering that in that case the pressure was obtained using the precipitating flux data measured for five energies only. But even in this case, the obtained correlation coefficient is very high. All of this means that the solar wind dynamic pressure directly influences the plasma pressure in the external part of the RC, which is related to the pressure balance at the magnetopause on the magnetospheric flanks. There exists a transition from the pressure balance supported by magnetic field of the Earth's dipole to the pressure balance of the solar wind dynamic pressure component acting to the magnetopause and plasma pressure inside the magnetosphere (Antonova et al., 2018).

3.3. Variation of the Plasma Pressure in the Maximum and the Influence of O^+ Ions

As mentioned before, the plasma pressure in the magnetosphere often reaches its maximum value at distances closer to the Earth than 6 R_E (see, e.g., the maximums in plasma pressure, obtained by the THEMIS

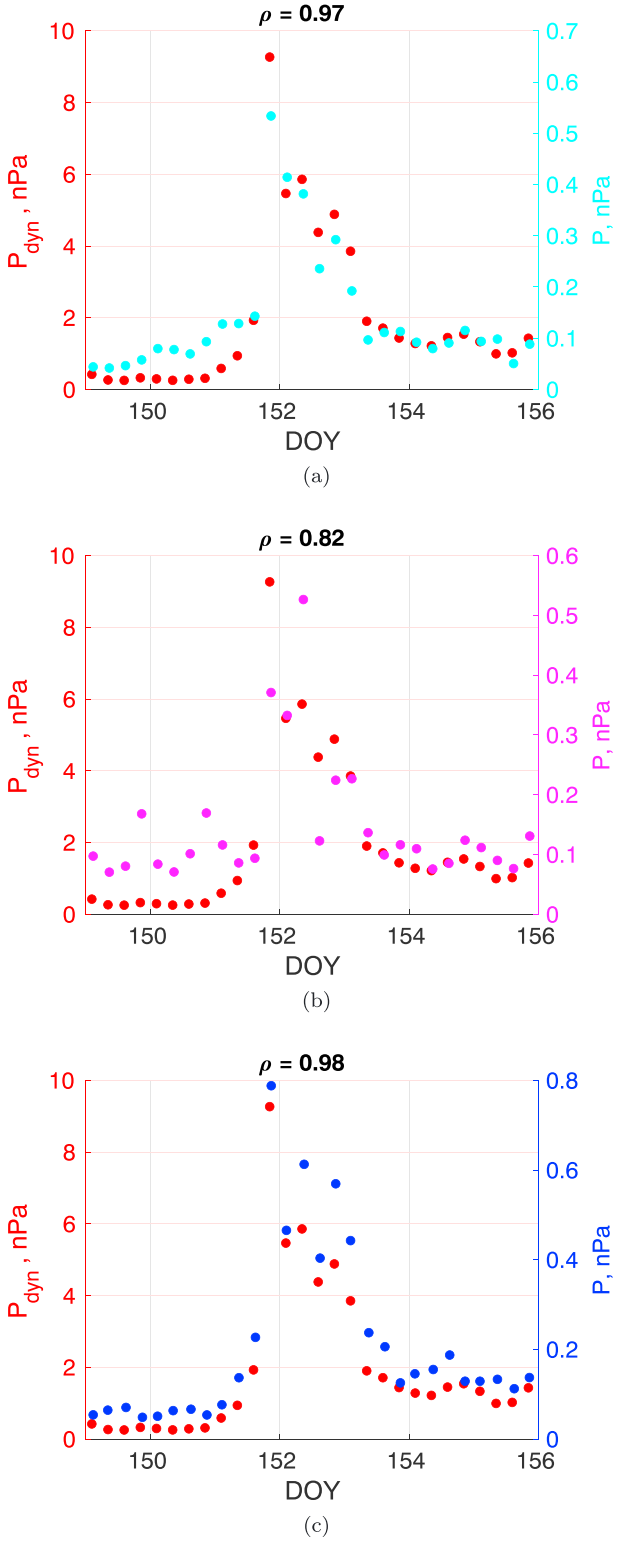

Figure 7. Correlation between the solar wind dynamic pressure (red) and the static pressure in the magnetosphere between 7 and 13 R_E, obtained using the data of Defense Meteorological Satellite Program (cyan, a), Polar Operational Environmental Satellites (magenta, b), and Time History of Events and Macroscale Interactions (blue, c) satellites. DOY = day of year.

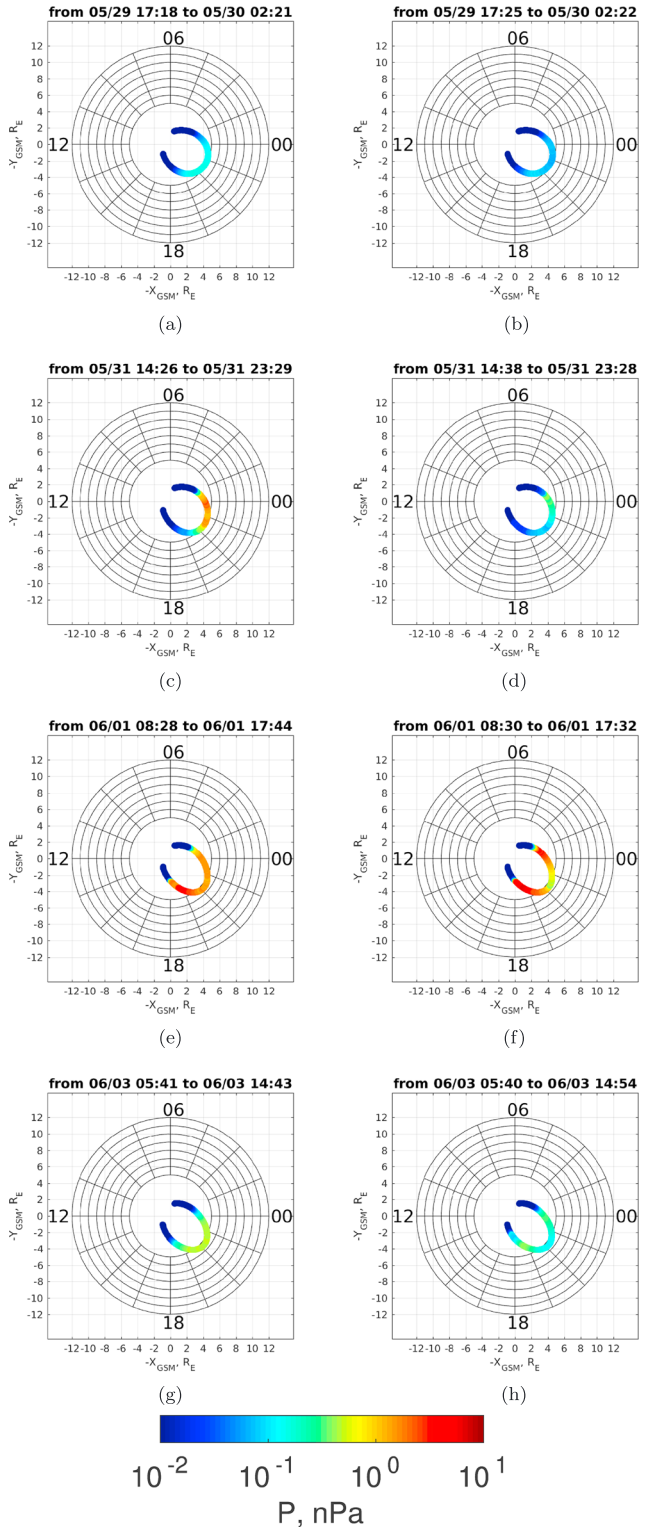

Figure 8. Variation of both proton (left column) and oxygen (right column) pressures along the Van Allen Probe B trajectory, obtained for the quiet time (a, b), a few hours before the main phase (c, d), during the main phase (e, f), and during the recovery phase (h, g). GSM = geocentric solar magnetospheric coordinates.

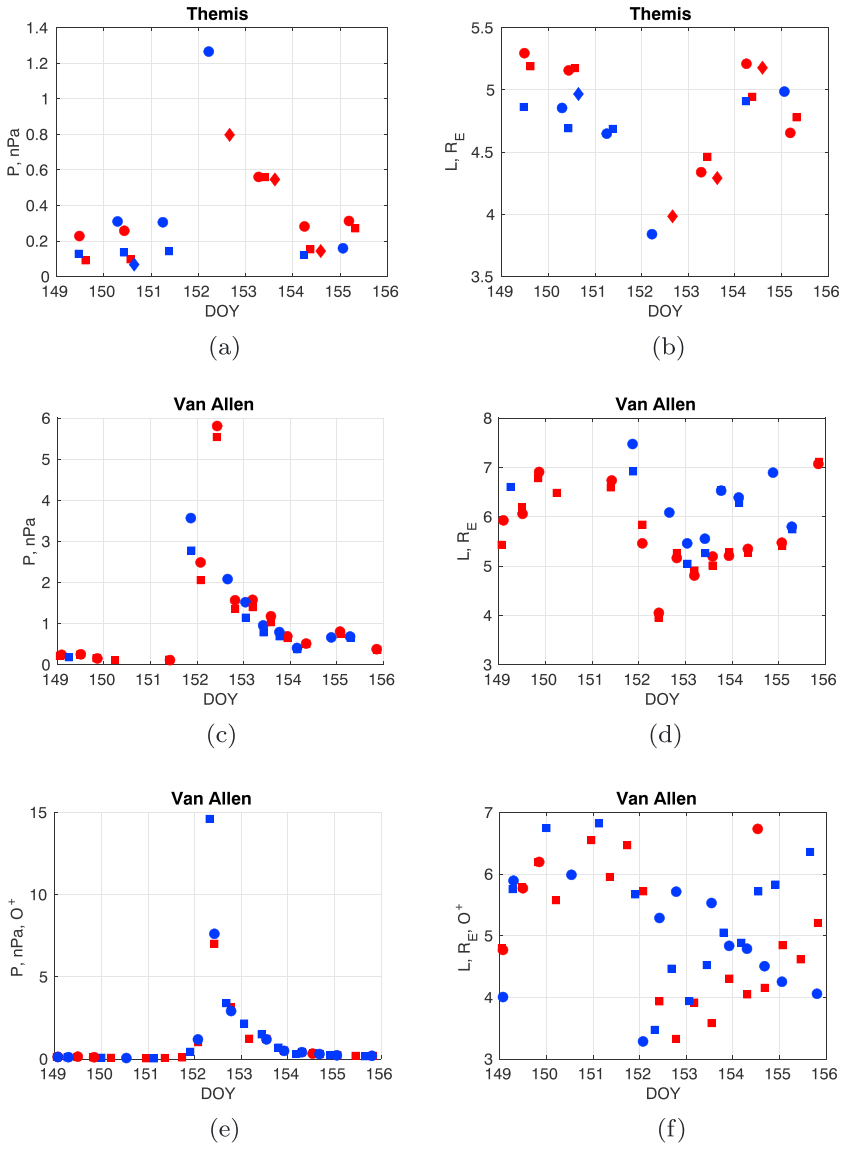

Figure 9. From top to bottom: Variation of the maximum proton pressure (a) and its respective location (b) measured by the THA (diamond), THD (circle), and THE (square) satellites. The same for the proton (c and d) and O^+ (f and g) pressures, measured by the RBSP-A (circle) and RBSP-B (square) satellites. For all satellites red symbol corresponds to the outbound orbit, and the blue symbol corresponds to the inbound orbit segment. DOY = day of year.

satellites in Figure 5). These distances were excluded from the analysis of the DMSP/POES data because of the following reasons: the plasma pressure could be anisotropic, the field-aligned potential drop could be strong, and the detectors could be affected by energetic particles. In this study we applied the automatic data analysis, so we restricted our statistical analysis to the region between 7 and 13 R_E. Nevertheless, we used the data from the THEMIS and Van Allen satellite missions to complement the statistical study and to determine how the maximum value of plasma pressure and its position change during the storm. It was done using the data of the THEMIS and Van Allen Probe missions (see Figures 5 and 8 for an overview). In case of the Van Allen Probes, it was done for both proton and O^+ ion pressure.

Figure 8 shows some examples of the variation of plasma pressure along the Van Allen Probe B satellite trajectory for protons (left column) and ions (right column) during quiet time, prestorm, and main and recovery phases. As it can be seen, during quiet times the contribution of O^+ into the total pressure was very low. It starts to drastically increase during the pre–storm time, and especially during the main phase, when the contribution of O^+ is predominant.

Figure 9 summarizes the proton pressure behavior during 1 June 2013 storm, obtained from THEMIS (a, b) and Van Allen Probes (c, d) during inbound (blue) and outbound (red) trajectories. As it can be seen, both missions show similar results. The maximum pressure increases with the storm development reaching the maximum value near ~ 6 nPa when the D_{st} index is minimum. The pressure generated by the O^+ has a similar behavior but reaches an even higher value of ~ 15 nPa, giving a value of ~ 20 nPa for the total plasma pressure. The position of the pressure maximum gradually moves closer to the Earth getting the minimum value of ~ 3.7–3.9 R_E. For both missions the L value was calculated by mapping the current satellite position into the geomagnetic equatorial plane as $\left(X^2+Y^2+Z^2\right)^{3/2}/\left(X^2+Y^2\right)$, assuming the dipole configuration. Both proton pressures measured using the data from the Van Allen Probes and the THEMIS satellites gave similar L value. Therefore, the azimuthal asymmetry was not strong. Finally, during the recovery phase an azimuthal asymmetry starts to appear, and the proton plasma pressure measured by the Van Allen Probes in the outbound and inbound orbits are slightly different. As a general trend, the maximums in plasma pressure for the Van Allen Probes orbits located closer to the magnetic midnight (blue symbols) were located at greater L. The same trend is observed for the O^+ satellite, but with greater dispersion.

4. Discussions

The behavior of plasma pressure during the 1 June 2013 geomagnetic storm can be analyzed in terms of the development of the RC under the condition of magnetostatic equilibrium. Tverskaia (1986) experimentally established that the position of the maximum of electron injections during a geomagnetic storm ($L_{\max}$) is related to the minimum in the D_{st} variation as $|D_{st,\min}| = cL_{\max}^{-4}$, with $c = 2.75 \cdot 10^4$. This relation was then explained in the theoretical works developed by Tverskoy (1997) and Antonova (2006). Later Antonova and Stepanova (2015) showed that this position at the same time coincides with the position in the pressure maximum and with the position of the auroral electrojet. For the 1 June 2013 storm analyzed here, the level of the solar wind dynamic pressure is high, reaching values near 10 nPa. This means that it is necessary to use the pressure-corrected D_{st}^* index as suggested by Burton et al. (1975). In the case of a 10-nPa pressure, the D_{st}^*=149 nT, and then, the Tverskaia (1986) relation predicts a value of $L_{\max} = 3.73$. This is in perfect agreement with $L \approx 3.7$–$3.9\ R_E$, obtained using the dipole approximation. The value of the total (proton plus O^+) pressure, which is about 20 nPa, agrees with both the observed minimum in the D_{st} variation and the predicted position of the pressure maximum. Thus, our results confirm the validity of the Tverskoy (1997) theory (see also ; Antonova, 2006). In addition, as opposite to the Dressler-Parker-Skopke relation, this model not only determines the value of the azimuthally symmetric magnetic field distortion at the Earth caused by the RC for large magnetic storms but also determines the position of the plasma pressure maximum during the magnetic storms. Such position determines the location of the maximum of the outer electron radiation belt formed after the storm (Antonova & Stepanova, 2015; Antonova et al., 2018; Moya et al., 2017; Tverskaya, 2011). Our results also confirm the contribution of the CRC to the D_{st} variation.

As it is shown in section 3.1, the plasma pressure in the plasma ring surrounding the Earth was changing and contributing to the change in is complementary to the ordinary RC and surrounds the Earth at geocentric distances of 7–10 R_E. The compression of the magnetic field lines at the dayside and the shift of the position of the minima of the magnetic field to higher latitudes lead to the spreading of the transverse current along field lines and to a splitting of the daytime integral transverse current into two branches. In magnetostatic equilibrium, it is possible to calculate the current density knowing the plasma pressure and magnetic field. Antonova et al. (2009) estimated the value of the transverse currents in the inner magnetosphere and showed that the total transverse current at the dayside field lines is comparable with the total transverse current near midnight at the same geocentric distances. This means that this current closes inside the magnetosphere, forming a high-latitude continuation of the ordinary RC (Antonova et al., 2018). The CRC has nearly the same topology as the traditional RC in the inner magnetospheric regions. The main difference between the CRC and the traditional RC is the nature of the main current carriers: plasma sheet-like particles (mainly ions with energies between 1 and 10 keV) in the case of CRC compared to ions with energies of the order of 100 keV in the case of RC. In our current study a direct comparison of plasma pressures, obtained by the low-orbiting DMSP and POES satellites near the Earth, and by the high-orbiting THEMIS satellites—for the segments of orbits located between 7 and 13 R_E—showed that the values of both pressures are very similar and vary in the same way during all phases of the storm, indicating that the major part of the auroral oval is mapped into the CRC region. For the segments of the THEMIS orbits and for the orbits of the Van Allen

Probes satellites located closer to the Earth, the observed values of pressure are much higher. In the case of THEMIS the maximum value of pressure reached 1.2 nPa, while for the Van Allen Probes it reached 6 nPa in the case of protons, and 15 nPa in the case of O^+, and mainly correspond to the RC region. This means that at the end of the main phase of the storm the proton pressure between 20 and 22 MLT was a few times higher than in the postmidnight and morning sectors. This result agrees with previous studies (see, e.g., Figure 10 of Zhang et al., 2007, showing the pressure distribution as a result of a global simulation).

It is important to mention that the B_z component of the IMF turned southward for nearly 7 hr during the main phase of the 1 June 2013 geomagnetic storm. The southward excursion of the IMF B_z is commonly associated with an increase in the [$\mathbf{V} \times \mathbf{B}$] electric field and increase in the reconnection rate at the dayside magnetopause, leading to the storm development. However, Antonova and Ganushkina (1997) showed that the dawn-dusk electric field can be created due to the closing of the Region I currents, and its intensification during the negative B_z can be explained by considering that the external magnetic field can penetrate directly to the magnetosphere leading to the alteration of the current systems. In case of the negative B_z this penetration leads to the intensification of the field-aligned currents (Antonova & Ganushkina, 1997) and hence to an increase of the dawn-dusk potential drop. Wing and Sibeck (1997) studied the influence of the B_z components of the IMF in combination with the solar wind dynamic pressure to the geomagnetic field measured at geosynchronous orbit. They found that an increase in the dynamic pressure depresses the geomagnetic field in the nightside and increases the geomagnetic field in the dayside. They also found that the southward IMF "penetrates" much stronger in comparison to the northward one. They attributed these effects to the intensification of the cross-tail and magnetopause currents. During the periods of the southward IMF, the B_x component of the geomagnetic field depends most strongly on the IMF B_z component, which was interpreted to the enhancement of the Region I field-aligned currents. From our point of view, these results can be interpreted in terms of the intensification of the field-aligned currents due to both the increase of plasma pressure gradients, and the depression of the geomagnetic field.

The intensification of the field-aligned currents leads to an increase of the field-aligned potential drop and hence to an increase in the flow of O^+ of ionospheric origin to the magnetosphere. The presence of O^+ provides a significant contribution to the plasma pressure and leads to the additional intensification of both transverse and field-aligned currents. In our case, during the minimum of the D_{st} variation, the contribution of O^+ into the total plasma pressure was more than 60%, which agrees with the previous results obtained by Kistler et al. (2016).

5. Conclusions

Our current study showed that the plasma pressure in the region of the RC, including the CRC, strongly changed during the 1 June 2013 geomagnetic storm. The 2-D distribution of the proton plasma pressure between 7 and 13 Earth's radii was obtained using the data of low-orbiting DMSP and POES satellites. It was found that this pressure changes significantly during the storm and did not show any significant azimuthal asymmetry. This distribution is not uniform and has a patchy character, which is in agreement with a local increase of pressure during substorm dipolarizations during storm time.

Simultaneous study of the proton plasma pressure made using the THEMIS satellite showed that between 7 and 13 R_E both missions gave similar values of pressure, indicating that the major part of the auroral oval is mapped into the CRC, introduced by Antonova and Ganushkina (1997) and Antonova (2004). At the same time, we found that the obtained plasma pressure using several spacecraft strongly correlates with the solar wind dynamic pressure with correlation coefficients exceeding 0.8.

The study of the behavior of the maximum value of plasma pressure showed that it increases during the main phase of the storm, reaching the maximum level when the D_{st} value is minimum, and at the same time the position of the maximum moves closer to Earth. The position of the obtained pressure maximum coincides with the L shell value predicted by the Tverskoy (1997) theory of the storm time plasma pressure disturbances. An interesting feature of the observed storm is a comparatively large increase of plasma pressure before the beginning of the storm in the CRC (the outer part of the ring current). This feature can be explained by the pressure balance at the magnetopause discussed by Antonova et al. (2018). Analysis of plasma pressure made using the Van Allen Probes satellite mission also revealed the significant contribution of O^+, consistent with the previous results of Kistler et al. (2016).

In summary, the analysis of the 1 June 2013 geomagnetic storm showed that the combination of the low- and high-orbiting measurements is very promising for the study of the behavior of plasma pressure in the inner magnetosphere. We propose to continue these studies by combining the satellite data analysis and modeling of the geomagnetic field, especially during strong geomagnetic storm events.

Acknowledgments
We acknowledge NASA contract NAS5-02099 and V. Angelopoulos for use of data from the THEMIS Mission. Specifically, C. W. Carlson and J. P. McFadden for use of ESA data, which can be downloaded from http://themis.ssl.berkeley.edu/data/themis/. The authors acknowledge JHU/APL for the use of the DMSP particle detectors data designed by Dave Hardy of AFRL. The DMPS SSJ/4 data can be downloaded from http://sd-www.jhuapl.edu/Aurora/data/data_step1.cgi. We also thank Herb Funsten, Ruth Skoug, Brian Larsen, and Geoff Reeves for the use of Van Allen Probes HOPE data, which can be downloaded from https://www.rbsp-ect.lanl.gov/science/DataDirectories.php. This work was supported by the Russian Foundation for Basic Research (RFBR; project 18-15-00362), Chilean FONDECYT 1161356 (M. S.), 11150055 (P. S. M.), 1150718 (J. A. V.) grants, CONICYT PIA Project "Anillo de Investigación en Ciencia y Tecnología" ACT1405, and CEDENNA under Conicyt Grant FB0807. V. A. Pinto would like to thank the support of Becas Chile fellowship program.

References

Angelopoulos, V. (2008). The THEMIS mission. *Space Science Reviews*, *141*(1-4), 5–34. https://doi.org/10.1007/s11214-008-9336-1

Antonova, E. E. (2004). Magnetostatic equilibrium and current systems in the Earth's magnetosphere. *Advances in Space Research*, *33*, 752–760. https://doi.org/10.1016/S0273-1177(03)00636-7

Antonova, E. E. (2006). Stability of the magnetospheric plasma pressure distribution and magnetospheric storms. *Advances in Space Research*, *38*, 1626–1630. https://doi.org/10.1016/j.asr.2005.05.005

Antonova, E. E., & Ganushkina, N. Y. (1997). Azimuthal hot plasma pressure gradients and dawn-dusk electric field formation. *Journal of Atmospheric and Solar-Terrestrial Physics*, *59*, 1343–1354. https://doi.org/10.1016/S1364-6826(96)00169-1

Antonova, E. E., & Kirpichev, I. P. (2014). Plasma pressure distribution in the surrounding the Earth plasma ring and its role in the magnetospheric dynamics. *Journal of Atmospheric and Solar-Terrestrial Physics*, *115*, 32–40. https://doi.org/10.1016/j.jastp.2013.12.005

Antonova, E. E., Kirpichev, I. P., Ovchinnikov, I. L., Orlova, K. G., & Stepanova, M. V. (2009). High latitude magnetospheric topology and magnetospheric substorm. *Annales Geophysicae*, *27*, 4069–4073. https://doi.org/10.5194/angeo-27-4069-2009

Antonova, E. E., Kirpichev, I. P., Vovchenko, V. V., Stepanova, M. V., Riazantseva, M. O., Pulinets, M. S., & Ovchinnikov, I. L. (2013). Characteristics of plasma ring, surrounding the Earth at geocentric distances ~ 7–10 $R_{E,}$ and magnetospheric current systems. *Journal of Atmospheric and Solar-Terrestrial Physics*, *99*, 85–91. https://doi.org/10.1016/j.jastp.2012.08.013

Antonova, E. E., & Stepanova, M. V. (2015). The problem of the acceleration of electrons of the outer radiation belt and magnetospheric substorms. *Earth, Planets, and Space*, *67*, 148. https://doi.org/10.1186/s40623-015-0319-7

Antonova, E. E., Stepanova, M., Kirpichev, I. P., Ovchinnikov, I. L., Vorobjev, V. G., Yagodkina, O. I., et al. (2018). Structure of magnetospheric current systems and mapping of high latitude magnetospheric regions to the ionosphere. *Journal of Atmospheric and Solar-Terrestrial Physics*, *177*, 103–114. https://doi.org/10.1016/j.jastp.2017.10.013

Antonova, E. E., Vorobjev, V. G., Kirpichev, I. P., & Yagodkina, O. I. (2014). Comparison of the plasma pressure distributions over the equatorial plane and at low altitudes under magnetically quiet conditions. *Geomagnetism and Aeronomy*, *54*, 278–281. https://doi.org/10.1134/S0016793214030025

Antonova, E. E., Vorobjev, V. G., Kirpichev, I. P., Yagodkina, O. I., & Stepanova, M. V. (2015). Problems with mapping the auroral oval and magnetospheric substorms. *Earth, Planets, and Space*, *67*, 166. https://doi.org/10.1186/s40623-015-0336-6

Burton, R. K., McPherron, R. L., & Russell, C. T. (1975). An empirical relationship between interplanetary conditions and Dst. *Journal of Geophysical Research*, *80*, 4204–4214. https://doi.org/10.1029/JA080i031p04204

Buzulukova, N., Fok, M.-C., Pulkkinen, A., Kuznetsova, M., Moore, T. E., Glocer, A., et al. (2010). Dynamics of ring current and electric fields in the inner magnetosphere during disturbed periods: CRCM-BATS-R-US coupled model. *Journal of Geophysical Research*, *115*, A05210. https://doi.org/10.1029/2009JA014621

De Michelis, P., Daglis, I. A., & Consolini, G. (1997). Average terrestrial ring current derived from AMPTE/CCE-CHEM measurements. *Journal of Geophysical Research*, *102*, 14,103–14,112. https://doi.org/10.1029/96JA03743

Denton, M. H., Jordanova, V. K., Henderson, M. G., Skoug, R. M., Thomsen, M. F., Pollock, C. J., et al. (2005). Storm-time plasma signatures observed by IMAGE/MENA and comparison with a global physics-based model. *Geophysical Research Letters*, *32*, L17102. https://doi.org/10.1029/2005GL023353

Ebihara, Y., & Fok, M.-C. (2004). Postmidnight storm-time enhancement of tens-of-keV proton flux. *Journal of Geophysical Research*, *109*, A12209. https://doi.org/10.1029/2004JA010523

Funsten, H. O., Skoug, R. M., Guthrie, A. A., MacDonald, E. A., Baldonado, J. R., Harper, R. W., et al. (2013). Helium, Oxygen, Proton, and Electron (HOPE) mass spectrometer for the Radiation Belt Storm Probes Mission. *Space Science Reviews*, *179*, 423–484. https://doi.org/10.1007/s11214-013-9968-7

Ganushkina, N. Y., Liemohn, M. W., & Dubyagin, S. (2018). Current systems in the Earth's magnetosphere. *Reviews of Geophysics*, *56*, 309–332. https://doi.org/10.1002/2017RG000590

Ganushkina, N. Y., Liemohn, M. W., Dubyagin, S., Daglis, I. A., Dandouras, I., De Zeeuw, D. L., et al. (2015). Defining and resolving current systems in geospace. *Annales Geophysicae*, *33*, 1369–1402. https://doi.org/10.5194/angeo-33-1369-2015

Ganushkina, N. Y., Liemohn, M. W., Kubyshkina, M. V., Ilie, R., & Singer, H. J. (2010). Distortions of the magnetic field by storm-time current systems in Earth's magnetosphere. *Annales Geophysicae*, *28*, 123–140. https://doi.org/10.5194/angeo-28-123-2010

Gkioulidou, M., Ukhorskiy, A. Y., Mitchell, D. G., & Lanzerotti, L. J. (2016). Storm time dynamics of ring current protons: Implications for the long-term energy budget in the inner magnetosphere. *Geophysical Research Letters*, *43*, 4736–4744. https://doi.org/10.1002/2016GL068013

Gkioulidou, M., Ukhorskiy, A. Y., Mitchell, D. G., Sotirelis, T., Mauk, B. H., & Lanzerotti, L. J. (2014). The role of small-scale ion injections in the buildup of Earth's ring current pressure: Van Allen Probes observations of the 17 March 2013 storm. *Journal of Geophysical Research: Space Physics*, *119*, 7327–7342. https://doi.org/10.1002/2014JA020096

Greenspan, M. E., & Hamilton, D. C. (2000). A test of the Dessler-Parker-Sckopke relation during magnetic storms. *Journal of Geophysical Research*, *105*, 5419–5430. https://doi.org/10.1029/1999JA000284

Keesee, A. M., & Scime, E. E. (2015). Database of ion temperature maps during geomagnetic storms. *Earth and Space Science*, *2*, 39–46. https://doi.org/10.1002/2014EA000061

Kirpichev, I. P., & Antonova, E. E. (2011). Plasma pressure distribution in the equatorial plane of the Earth's magnetosphere at geocentric distances of 6–10 R_E according to the international THEMIS mission data. *Geomagnetism and Aeronomy*, *51*, 450–455. https://doi.org/10.1134/S0016793211040049

Kistler, L. M., Mouikis, C. G., Spence, H. E., Menz, A. M., Skoug, R. M., Funsten, H. O., et al. (2016). The source of O^+ in the storm time ring current. *Journal of Geophysical Research: Space Physics*, *121*, 5333–5349. https://doi.org/10.1002/2015JA022204

Liemohn, M. W., Kozyra, J. U., Clauer, C. R., & Ridley, A. J. (2001). Computational analysis of the near-Earth magnetospheric current system during two-phase decay storms. *Journal of Geophysical Research*, *106*, 29,531–29,542. https://doi.org/10.1029/2001JA000045

Lui, A. T. Y., & Hamilton, D. C. (1992). Radial profiles of quiet time magnetospheric parameters. *Journal of Geophysical Research*, *97*, 19,325–19,332. https://doi.org/10.1029/92JA01539

Mauk, B., Fox, N., Kanekal, S., Kessel, R., Sibeck, D., & Ukhorskiy, A. (2012). Science objectives and rationale for the Radiation Belt Storm Probes mission. *Space Science Reviews*, *179*, 1–25. https://doi.org/10.1007/s11214-012-9908-y

McFadden, J. P., Carlson, C. W., Larson, D., Bonnell, J., Mozer, F., Angelopoulos, V., et al. (2008). THEMIS ESA first science results and performance issues. *Space Science Reviews*, *141*, 477–508. https://doi.org/10.1007/s11214-008-9433-1

Moya, P. S., Pinto, V. A., Sibeck, D. G., Kanekal, S. G., & Baker, D. N. (2017). On the effect of geomagnetic storms on relativistic electrons in the outer radiation belt: Van Allen Probes observations. *Journal of Geophysical Research: Space Physics*, *122*, 11,100–11,108. https://doi.org/10.1002/2017JA024735

Spence, H. E., Reeves, G. D., Baker, D. N., Blake, J. B., Bolton, M., Bourdarie, S., et al. (2013). Science goals and overview of the Radiation Belt Storm Probes (RBSP) Energetic Particle, Composition, and Thermal Plasma (ECT) suite on NASA's Van Allen Probes mission. *Space Science Reviews*, *179*, 311–336. https://doi.org/10.1007/s11214-013-0007-5

Stepanova, M., Antonova, E. E., & Bosqued, J.-M. (2006). Study of plasma pressure distribution in the inner magnetosphere using low-altitude satellites and its importance for the large-scale magnetospheric dynamics. *Advances in Space Research*, *38*, 1631–1636. https://doi.org/10.1016/j.asr.2006.05.013

Stepanova, M., Antonova, E. E., & Bosqued, J. M. (2008). Radial distribution of the inner magnetosphere plasma pressure using low-altitude satellite data during geomagnetic storm: The March 1–8, 1982 event. *Advances in Space Research*, *41*, 1658–1665. https://doi.org/10.1016/j.asr.2007.06.002

Stepanova, M. V., Antonova, E. E., Bosqued, J. M., & Kovrazhkin, R. (2004). Radial plasma pressure gradients in the high latitude magnetosphere as sources of instabilities leading to the substorm onset. *Advances in Space Research*, *33*, 761–768. https://doi.org/10.1016/S0273-1177(03)00634-3

Stepanova, M. V., Antonova, E. E., Bosqued, J. M., Kovrazhkin, R. A., & Aubel, K. R. (2002). Asymmetry of auroral electron precipitations and its relationship to the substorm expansion phase onset. *Journal of Geophysical Research*, *107*, 1134. https://doi.org/10.1029/2001JA003503

Tverskaia, L. V. (1986). The boundary of electron injection into the Earth magnetosphere. *Geomagnetism and Aeronomy*, *26*, 864.

Tverskaya, L. V. (2011). Diagnostics of the magnetosphere based on the outer belt relativistic electrons and penetration of solar protons: A review. *Geomagnetism and Aeronomy*, *51*, 6–22. https://doi.org/10.1134/S0016793211010142

Tverskoy, B. A. (1997). Formation mechanism for the structure of the magnetic storm ring current. *Geomagnetism and Aeronomy (In Russian)*, *37*, 555–559.

Wang, C.-P., Gkioulidou, M., Lyons, L. R., Wolf, R. A., Angelopoulos, V., Nagai, T., et al. (2011). Spatial distributions of ions and electrons from the plasma sheet to the inner magnetosphere: Comparisons between THEMIS-Geotail statistical results and the Rice convection model. *Journal of Geophysical Research*, *116*, A11216. https://doi.org/10.1029/2011JA016809

Wing, S., Gkioulidou, M., Johnson, J. R., Newell, P. T., & Wang, C.-P. (2013). Auroral particle precipitation characterized by the substorm cycle. *Journal of Geophysical Research: Space Physics*, *118*, 1022–1039. https://doi.org/10.1002/jgra.50160

Wing, S., & Newell, P. T. (1998). Central plasma sheet ion properties as inferred from ionospheric observations. *Journal of Geophysical Research*, *103*, 6785–6800. https://doi.org/10.1029/97JA02994

Wing, S., & Newell, P. T. (2000). Quiet time plasma sheet ion pressure contribution to Birkeland currents. *Journal of Geophysical Research*, *105*, 7793–7802. https://doi.org/10.1029/1999JA900464

Wing, S., & Sibeck, D. G. (1997). Effects of interplanetary magnetic field z component and the solar wind dynamic pressure on the geosynchronous magnetic field. *Journal of Geophysical Research*, *102*, 7207–7216. https://doi.org/10.1029/97JA00150

Zaharia, S., Thomsen, M. F., Birn, J., Denton, M. H., Jordanova, V. K., & Cheng, C. Z. (2005). Effect of storm-time plasma pressure on the magnetic field in the inner magnetosphere. *Geophysical Research Letters*, *32*, L03102. https://doi.org/10.1029/2004GL021491

Zhang, J., Liemohn, M. W., de Zeeuw, D. L., Borovsky, J. E., Ridley, A. J., Toth, G., et al. (2007). Understanding storm-time ring current development through data-model comparisons of a moderate storm. *Journal of Geophysical Research*, *112*, A04208. https://doi.org/10.1029/2006JA011846

Zhao, H., Li, X., Baker, D. N., Claudepierre, S. G., Fennell, J. F., Blake, J. B., et al. (2016). Ring current electron dynamics during geomagnetic storms based on the Van Allen Probes measurements. *Journal of Geophysical Research: Space Physics*, *121*, 3333–3346. https://doi.org/10.1002/2016JA022358

Zhao, H., Li, X., Baker, D. N., Fennell, J. F., Blake, J. B., Larsen, B. A., et al. (2015). The evolution of ring current ion energy density and energy content during geomagnetic storms based on Van Allen Probes measurements. *Journal of Geophysical Research: Space Physics*, *120*, 7493–7511. https://doi.org/10.1002/2015JA021533